Quantum vortices in a glass of Bose-Einstein condensate

Nicolas Grisouard

1 Introduction

Bose-Einstein condensation occurs for bosons when, for a temperature low enough (typically a few kelvins for a liquid condensate and a few nanokelvins for a gaseous condensate), a macroscopic fraction[1] of the bosons gathers in the quantum state of lowest energy, forming a Bose-Einstein condensate (BEC). In this case, the behavior of the fluid can be described in the case of a dilute gas by the nonlinear Schrödinger equation (NLS), also called the Gross-Pitaevskii equation. It can be shown that the dynamics of the NLS is very close to shallow water dynamics with surface tension. One of the striking features of BECs is the possibility of point vortices to appear, which dynamics is explained in some the oldest textbooks of fluid dynamics (see *e.g.* [5]). Surprinsingly, although vortices in BECs have been extensively studied, some of the most simple *Gendankenexperiments* have yet to be studied. In [6] for example, the (apparently) simple problem of the motion of a single vortex along a plane boundary in a semi-infinite, uniform BEC is studied, eleven years after the first experimental realisation of a BEC ([3]) and eighty-two years after Einstein's translation of the letter Bose wrote him about what would later be called Bose-Einstein statistics ([1]). An opportunity is then to be seized by classical fluid dynamicists, who can make the study of quantum fluid dynamics benefit from their experience. The idea of the present project, unlike [6] who use an almost all-analytical approach, is to develop a numerical code to integrate the NLS in polar coordinates and to perform a few numerical experiments about vortices in a two-dimensional circular box (a "glass"). In this report, we will first present some aspects of quantum fluid dynamics for geophysical fluid dynamicists to understand the analogies between the two fields. The code written during the project will then be presented in Section 3. In Section 4, a few numerical experiments will be presented to validate the code, study various simple configurations and see what the code can do. In a last section, conclusions will be drawn and possible extensions of this work will be proposed.

2 Two-dimensional Bose-Einstein condensates

2.1 The nonlinear Schrödinger equation

In a dilute gas of N particles, each particle barely interacts with the others and in first approximation, its wave function does not feel the presence of the other particles. In this case, it is possible to approximate the total wave function Ψ as the product of all the

[1] to be understood as a fraction not involving negative powers of ten

individual wave functions $\widetilde{\psi}_i$:

$$\Psi(\boldsymbol{r_1}, \boldsymbol{r_2}, \ldots, t) = \prod_{i=1}^{N} \widetilde{\psi}_i(\boldsymbol{r_i}, t).$$

As the particles are all identical and in the same fundamental state, all $\widetilde{\psi}_i$ have the same form which we can write as

$$\widetilde{\psi}_i(\boldsymbol{r_i}, t) = \frac{\psi(\boldsymbol{r_i}, t)}{\sqrt{N}}.$$

The reason why we chose this particular scaling is that the normalization relation, which is that the probability of finding the i^{th} particle in the whole physical domain $\mathcal{D}$ is equal to 1, can be written as

$$\int_S |\psi|^2 \, dS = N. \tag{1}$$

Therefore, $|\psi|^2$ can be considered as the particle density.

We mentioned earlier that the particles barely interact with each other. In a dilute gas, this approximation is accurate but let us refine this model by introducing the fact that these particles indeed never interact except when their positions exactly coincide (collisions), in which case they feel a repulsive interaction. The hamiltonian of the system is therefore

$$H = \sum_{i=1}^{N} \left(-\frac{\hbar^2}{2m} \boldsymbol{\nabla}_i^2 + V(\boldsymbol{r}_i) \right) + \frac{1}{2} \sum_{i<j} U_0 \delta(\boldsymbol{r}_i - \boldsymbol{r}_j),$$

where $\hbar$ is the reduced Planck constant[2], m is the mass of a single particle, $V(\boldsymbol{r}_i)$ is the external energy potential and $\boldsymbol{\nabla_i}$ is the gradient operator relative to the set of coordinates $\boldsymbol{r_i}$. Integration of $\psi^* H \psi$ across the whole domain (where * means complex conjugate) gives the energy of the system:

$$E = \int_S \left(\frac{\hbar^2}{2m} |\boldsymbol{\nabla}\psi|^2 + V(\boldsymbol{r})|\psi|^2 + \frac{1}{2} U_0 |\psi|^4 \right) dx \, dy, \tag{2}$$

The wave function minimizes E under the constraint of Equation (1) and satisfies the NLS:

$$i\hbar \frac{\partial \psi}{\partial t} = \left[-\frac{\hbar^2}{2m} \boldsymbol{\nabla}^2 \psi + V(x, y) \right] \psi + U_0 |\psi|^2 \psi, \tag{3}$$

which entirely describes the dynamics of the BEC. The first term of the right member is the usual Schrödinger equation and the last term is the one introduced by the interaction terms, which is also the nonlinear term. In our case, we will consider a two-dimensional circular glass of radius R associated with a set of polar coordinates (r, θ) which origin lies in the center, in other words:

$$V(r \geq R, \theta) = +\infty, \qquad V(r < R, \theta) = V \text{ (constant)}.$$

In this case, the probability of finding a particle outside the glass is strictly equal to zero and we will therefore only focus on the interior of it.

[2] $\hbar \simeq 1.054571628 \times 10^{-34}$ J.s

2.2 The Madelung transformation

Before looking at the behavior of the NLS solutions, it might be useful for the reader who is more used to geophysical fluid dynamics to see how the dynamics of the NLS equation can seem familiar. ψ written in its polar form is

$$\psi(\boldsymbol{r},t) = \sqrt{n(\boldsymbol{r},t)}e^{i\alpha(\boldsymbol{r},t)}.$$

In this case, n and α are real, n is positive and can be easily interpreted as the particle density, as implied by Equation (1):

$$n(\boldsymbol{r},t) = |\psi(\boldsymbol{r},t)|^2.$$

Now multiplying Equation (3) by ψ^* and adding the result to its complex conjugate, one finds that n indeed satisfies a conservation law:

$$\frac{\partial n}{\partial t} = \frac{i\hbar}{2m}(\psi^*\boldsymbol{\nabla}^2\psi - \psi\boldsymbol{\nabla}^2\psi^*) = -\boldsymbol{\nabla}\cdot\boldsymbol{j},$$

with $\boldsymbol{j} = -(i\hbar/2m)(\psi^*\boldsymbol{\nabla}\psi - \psi\boldsymbol{\nabla}\psi)$ is the probability current also written as

$$\boldsymbol{j} = \frac{\hbar}{m}\Im(\psi^*\boldsymbol{\nabla}\psi) = \frac{\hbar}{m}n\boldsymbol{\nabla}\alpha.$$

A velocity vector can be defined such that $\boldsymbol{j} = n\boldsymbol{u}$, or

$$\boldsymbol{u} = \frac{\hbar}{m}\boldsymbol{\nabla}\alpha = \frac{\hbar}{m}\frac{\Im(\psi^*\boldsymbol{\nabla}\psi)}{n}.$$

As $\boldsymbol{u}$ is a gradient, we have $\boldsymbol{\nabla}\times\boldsymbol{u} = 0$, *i.e.* the flow is irrotationnal. Equation (4) is then

$$\partial_t n + \boldsymbol{\nabla}\cdot(n\boldsymbol{u}) = 0, \tag{4}$$

which is formally identical to the continuity equation in fluid dynamics. It is also possible to derive an equation similar to the Euler equations, although we will restrict ourselves to just mentioning it in the general case $\boldsymbol{\nabla}V \neq 0$:

$$\frac{D\boldsymbol{u}}{Dt} = -\frac{1}{m}\boldsymbol{\nabla}V - U_0\boldsymbol{\nabla}n + \frac{\hbar^2}{2m^2}\boldsymbol{\nabla}\left\{\frac{\boldsymbol{\nabla}^2(\sqrt{n})}{\sqrt{n}}\right\}. \tag{5}$$

The similarity to the Euler equations in classical fluid dynamics is made clearer when writing it in the following form:

$$\frac{D\boldsymbol{u}}{Dt} = -\boldsymbol{\nabla}\Phi - g\boldsymbol{\nabla}\eta + \frac{\sigma}{\rho}\boldsymbol{\nabla}\left\{\frac{\boldsymbol{\nabla}^2\eta}{(1+|\boldsymbol{\nabla}\eta|^2)^{3/2}}\right\},$$

where Φ is the potential of the external conservative forces acting on the fluid other than gravity, η the free-surface height, ρ the density and σ the surface tension. The term $-\boldsymbol{\nabla}\Phi$ is related to $-\boldsymbol{\nabla}V$ in Equation (5). The hydrostatic pressure gradient $-g\boldsymbol{\nabla}\eta$ is related to $-U_0\boldsymbol{\nabla}n$ which would be absent of Equation (5) if U_0 would be zero: the action of the nonlinear effects is then to avoid high concentrations of particles and "flatten" the particle

distribution, like pressure does for the height of a fluid surface. One can also notice that now, n is not related to ρ but to η. Finally, the last term of Equation (5), although not formally identical, can be related to the surface tension term of the last equation. Effects on the dynamics of the distribution of the particle density that are similar to those induced by surface tension at the surface of a fluid will be involved throughout this report, the most striking feature being the existence of density waves that behave like surface capillary-gravity waves in a classical fluid. As a remark, the flow can be compressible.

2.3 Non-dimensional problem

Before writing the NLS in a non-dimensional form, we first have to define characteristic quantities.

2.3.1 A characteristic length: the healing length

We have noticed in Section 2.2 that the nonlinear effects tend to homogenize the particle distribution. But the external potential is such that the wave function vanishes at the boundary of the domain. In the steady state, the particle density must therefore experience an evolution between the boundary condition and the interior of the BEC, this evolution being given by the steady NLS. For simplicity reasons, we consider here a plane, infinite wall which boundary lies along the y axis. We then have $\psi \equiv 0$ for $x \leq 0$ and the steady NLS is now

$$-\frac{\hbar^2}{2m}\frac{d^2\psi}{dx^2} + V\psi + U_0\psi^3 = 0. \tag{6}$$

This ODE is somehow similar to the following ODE:

$$\frac{1}{2}f'' + f - f^3 = 0,$$

which solution is the tanh function. In order to put Equation (6) in a similar form, we write $\psi = \sqrt{n_0}\hat{\psi}$ where n_0 is the background density away from the boundary and $\hat{\psi}$ is the dimensionless wave function. We also set $V = -U_0 n_0$, the external potential being now a direct result of all the individual interactions acting as a mean-field. Equation (6) becomes

$$-\frac{\hbar^2}{2mU_0n_0}\frac{d^2\hat{\psi}}{dx^2} + \hat{\psi} - \hat{\psi}^3 = 0.$$

The solution to this equation is then $\hat{\psi} = \tanh\left(x/(\sqrt{2}\xi)\right)$ where

$$\xi = \frac{\hbar}{\sqrt{2mn_0U_0}}. \tag{7}$$

ξ is the healing length and will be our characteristic length. As shown in Figure 1, $\xi\sqrt{2}$ is the typical distance on which the density relaxes from zero at the boundary to its background value n_0. We see again an action of the nonlinear term: without it, the ODE to solve would simply be the equation of an harmonic oscillator and the solutions would be the eigenmodes one finds for free particles trapped in a box, exhibiting oscillatory behaviors. We see as in Section 2.2 that the particle density is flattened by the extra term brought by the interactions between particles.

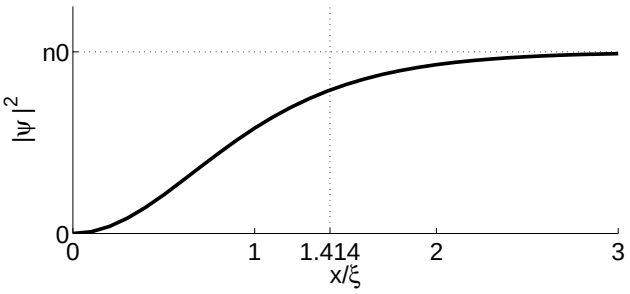

Figure 1: Particle density at rest from the boundary in $x = 0$ to its background density n_0.

2.3.2 Non-dimensional variables, non-dimensional NLS and invariants

We can now define a full set of non-dimensional variables by scaling length by ξ, time by $m\xi^2/\hbar$ and wave function by $\sqrt{n_0}$. By doing so and keeping $V = -n_0 U_0$ in the interior of the box, we get the non-dimensional version of the NLS:

$$\frac{\partial \psi}{\partial t} = \frac{i}{2}\boldsymbol{\nabla}^2\psi + \frac{i}{2}\left(1 - |\psi|^2\right)\psi. \tag{8}$$

We dropped the hat for the non-dimensional wave function. Scaling energy by $n_0\hbar^2/m$, Equation (2) can be written in a non-dimensional form:

$$E = \frac{1}{2}\int_S \left(|\boldsymbol{\nabla}\psi|^2 - |\psi|^2 + \frac{1}{2}|\psi|^4\right) dS.$$

In our two-dimensional, polar symmetry, the energy can be written as

$$E = \frac{1}{2}\int_0^{2\pi}\int_0^R \left(r\left|\frac{\partial\psi}{\partial r}\right|^2 + \frac{1}{r}\left|\frac{\partial\psi}{\partial\theta}\right|^2 - r|\psi|^2 + \frac{r}{2}|\psi|^4\right) dr\, d\theta.$$

We have derived two invariants so far, the number of particles N and the total energy E. A third invariant, the total angular momentum L, can be defined as

$$\boldsymbol{L} = \int_S \psi^*(-i\,\boldsymbol{r}\times\boldsymbol{\nabla})\psi\, dS$$

The only non-zero component of $\boldsymbol{L}$ being the one normal to the (r,θ) plane, we have

$$L = -i\int_0^{2\pi}\int_0^R \psi^*\frac{\partial\psi}{\partial\theta}\, r\, dr\, d\theta,$$

which is our third invariant.

Finally, the velocity can be made non-dimensional by scaling it by $\hbar/(m\xi)$. Its non-dimensional definition then simply becomes

$$\boldsymbol{u} = \boldsymbol{\nabla}\alpha.$$

2.4 Solutions of the nonlinear Schrödinger equation

2.4.1 Waves

Let us study the wave spectrum of the NLS for small perturbations relative to an uniform basic state of density $n_0 = 1$ with no mean velocity of the BEC:

$$\psi = 1 + \phi \quad \text{with} \quad |\phi| \ll 1.$$

Equation (8) becomes

$$\begin{aligned}\frac{\partial \phi}{\partial t} &= \frac{i}{2}\boldsymbol{\nabla}^2\phi - \frac{i}{2}\left(\phi + \phi^* + |\phi|^2\right)(1+\phi) \\ &= \frac{i}{2}\boldsymbol{\nabla}^2\phi - i\frac{\phi+\phi^*}{2} + O(|\phi|^2).\end{aligned}$$

Neglecting high-order terms and taking the complex conjugate of the previous expression gives the following system

$$\begin{cases} \dfrac{\partial \phi}{\partial t} = \dfrac{i}{2}\boldsymbol{\nabla}^2\phi - i\dfrac{\phi+\phi^*}{2}, \\ \dfrac{\partial \phi^*}{\partial t} = -\dfrac{i}{2}\boldsymbol{\nabla}^2\phi^* + i\dfrac{\phi^*+\phi}{2}. \end{cases}$$

We can rewrite the previous system as a linear matrix equation

$$\frac{\partial}{\partial t}\begin{bmatrix} \phi \\ \phi^* \end{bmatrix} = M \begin{bmatrix} \phi \\ \phi^* \end{bmatrix} \qquad \text{with} \quad M = \frac{i}{2}\begin{bmatrix} \boldsymbol{\nabla}^2 - 1 & -1 \\ 1 & 1 - \boldsymbol{\nabla}^2 \end{bmatrix}. \tag{9}$$

Let the solution be assumed to oscillate at frequency ω and let $[u, v]e^{-i\omega t}$ be the eigenvector of M associated with the eigenvalue $-i\omega$. As we will see in Section 3, the normal modes to use in polar coordinates are $u, v \sim e^{in\theta}J_n(kr)$ and as[3] $\boldsymbol{\nabla}^2(e^{in\theta}J_n(kr)) = -k^2 e^{in\theta}J_n(kr)$, Equation (9) is now

$$(M + i\omega)\begin{bmatrix} u \\ v \end{bmatrix} = \frac{i}{2}\begin{bmatrix} -k^2 - 1 + 2\omega & -1 \\ 1 & 1 + k^2 + 2\omega \end{bmatrix}\begin{bmatrix} u \\ v \end{bmatrix} = 0. \tag{10}$$

For this system to have a non-trivial solution, its determinant has to be zero, which yields the dispersion relation

$$\omega^2 = \frac{k^2}{2} + \frac{k^4}{4}.$$

This dispersion relation is formally similar to the dispersion relation of gravity-capillary waves in shallow water which reads (in dimensional units)

$$\omega^2 = gH|\boldsymbol{k}|^2 + \frac{\sigma H}{\rho}|\boldsymbol{k}|^4,$$

with H the mean water height. The first term in Equation (2.4.1) is a non-dispersive term due to the nonlinear term of the NLS. In the long-wave approximation ($k \to 0$), it is dominant and the dispersion relation is similar to the dispersion relation of long gravity waves or of acoustic waves. The second term becomes significant for shorter waves and in such a case, the waves disperse like gravity-capillary waves with short waves traveling faster than long waves. A visual comparison can easily be made in Figure 2.

[3] in polar coordinates, this equation is in fact the Bessel equation of order n multiplied by $e^{in\theta}$

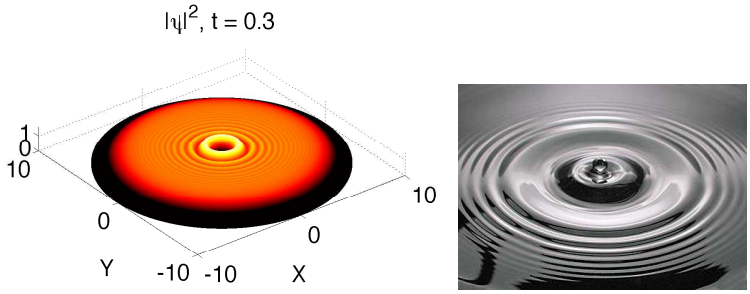

(a) Waves in a BEC (b) Water waves

Figure 2: Density waves in a BEC (a) compared with gravity-capillary waves in (deep) water (b). Due to the dispersion relation, short waves travel faster than long waves. The initial condition for the wave function used in picture (a) is $\psi = e^{i\theta}\tanh((R-r)/\sqrt{2})$ in the code described in Section 3 and the waves are created by the transient.

2.4.2 Vortices

We noticed in Section 2.2 that the flow was intrinsically irrotational. Writing that, we neglected possible singularities that could make the flow rotational on these points and we will see on an example how and why it is the case. Let us suppose that locally, the wave function can be written as

$$\psi = x + iy = r\exp(i\theta). \tag{11}$$

In this case, the wave function has a zero in $r = 0$ where the density vanishes. The velocity is then

$$\boldsymbol{u} = \boldsymbol{\nabla}\theta = \frac{1}{r}\hat{\boldsymbol{\theta}}.$$

In classical fluid dynamics, this velocity field would be the one induced by a point vortex inducing a divergence of the azimuthal velocity when $r \to 0$, which would be regularized giving some spatial extent to the core of the vortex. Here, this singularity is a fundamental feature of the field and it is required that these zeros are points and not lines or surfaces, as a result of the cancellation of both real and imaginary parts. It is also required that these two components cancel along lines and that these lines cross only on points. Take for example $\psi = x + ix$: this function admits a line of zeros defined by $x = 0$ where both real and imaginary parts cancel but no velocity is induced by it. If we take the simple example described by Equation (11), use Stoke's theorem to rewrite the circulation and compute the circulation of the velocity field around the origin, we get:

$$\Gamma = \oint_{\mathcal{C}} \boldsymbol{u}\cdot\boldsymbol{dr} = \iint_S (\boldsymbol{\nabla}\times\boldsymbol{\nabla}\theta)\cdot d\boldsymbol{S} = 2\pi.$$

Two things have to be noticed here. First, that the circulation is quantized. In general, for any vortex, it can only be an element of $\{2\pi p,\ p\in\mathbb{Z}\}$ ($\{2\pi p\hbar/m,\ p\in\mathbb{Z}\}$ in dimensional units). Second, that although Equation (11) looks harmless, a singularity is hidden at the origin as the phase is multivalued, which makes the quantity $\boldsymbol{\nabla}\times\boldsymbol{\nabla}\theta$ infinite in just one point.

One can wonder how far Equation (11) is a realistic expression for a vortex. A more refined but still approximate expression for the density structure around a steady point vortex is $|\psi|^2(r) = r^2/(r^2+1)$ (see *e.g.* [2]), so Equation (11) is a good approximation in the center of this vortex. One might also want to push the robustness of this feature and see what happens when the density around the vortex is perturbed. Let us consider a simple perturbation for the wave function:

$$\psi(x,y) = x + i(a_1 x + a_2 y). \tag{12}$$

The corresponding density is

$$n(x,y) = (1+a_1^2)\,x^2 + 2\,a_1 a_2\,xy + b_2\,y^2$$

and the lines of constant density are now ellipses. In polar coordinates ($x = r\cos\theta$, $y = r\sin\theta$), the wave function reads:

$$\psi(r,\theta) = r(\cos\theta + i(a_1\cos\theta + a_2\sin\theta))$$

and its phase is

$$\alpha = \arctan(a_1 + a_2\tan\theta),$$

which does not depend on r. This means that the radial velocity will be zero and the velocity will then be purely azimuthal, just like for the undisturbed vortex. As far as we know, this peculiar feature has surprisingly never been noticed. The azimuthal velocity is then

$$\begin{aligned} u_\theta(r,\theta) &= \frac{1}{r}\frac{\partial\alpha}{\partial\theta} = \frac{1}{r}\frac{a_2^2}{\cos^2\theta + (a_1\cos\theta + a_2\cos\theta)^2} \\ &= \frac{a_2^2\,r}{n(r,\theta)}. \end{aligned}$$

For a given r, the azimuthal velocity is maximum where the density is minimum, which is due to the conservation of the number of particles.

We have reviewed all the physical phenomena involved in this study. We will now describe the code that has been developed in order to perform simple numerical experiments.

3 The code

3.1 Operator splitting method

Operator splitting methods [4] are commonly used to solve the NLS, mostly because they are simple to implement in that case. The general idea is that the resolution of the NLS is splitted in two steps, starting from a time t:

[4] see *e.g.* [7]

Step 1: integration of $\psi(r,\theta,t)$ through equation

$$\frac{\partial \psi}{\partial t} = \frac{i\left(1-|\psi|^2\right)}{2}\psi$$

over a time step dt. As the variation of ψ is equal to $iK\psi$ where K is real, $|\psi|$ remains unchanged under this operation and the integration is then exact. After this step, we get an intermediate ψ_{int}:

$$\psi_{int}(r,\theta) = \psi(r,\theta,t)\exp\left(\frac{i(1-|\psi(r,\theta,t)|^2)dt}{2}\right).$$

Step 2: integration of $\psi_{int}(r,\theta)$ through equation

$$\frac{\partial \psi}{\partial t} = \frac{i}{2}\boldsymbol{\nabla}^2\psi \tag{13}$$

over a time step dt. If the integration is performed in the spectral space, this step is also exact and gives $\psi(r,\theta,t+dt)$. It will be explained in more detail in the next section.

As a remark, both steps are *individually* exact and energy preserving, although this will be discussed for the second step, but the combination of the two is not, therefore we need to choose dt small enough. A time step of $dt = 5\times10^{-3}$ ensures the stability of all simulations presented here.

3.2 Integrating the Laplacian

We here solve Equation (13) with ψ_{int} as initial condition for the wave function. In polar coordinates, this function can be decomposed as

$$\psi_{int} = \sum_{q=-\infty}^{+\infty}\sum_{j=1}^{+\infty}(a_{q,j})_{int}\, e^{iq\theta}\, J_q(k_{q,j}r). \tag{14}$$

Here, q is the index of the angular mode, j the index of the radial mode, J_q the q^{th}-order Bessel function of the first kind and $k_{q,j}$ a coefficient scaling J_q such that $\forall(q,j)$, $J_q(k_{q,j}R) = 0$ (which ensures that $\psi_{int}(r=R,\theta)\equiv 0$). The index j is therefore the number of zeros in the interval $[0,R]$ of the considered Bessel function (see Figure 3 for a visualization of various $J_q(k_{q,j}r)$'s). Finally, the set of $a_{q,j}$ is the set of weights that will characterize ψ_{int} and therefore depend on time. It turns out that applying the Laplacian to Equation (14) gives the Bessel equation and as in Section 2.4.1, we get:

$$\boldsymbol{\nabla}^2\psi_{int} = -\sum_{q=-\infty}^{+\infty}\sum_{j=1}^{+\infty}k_{q,j}^2(a_{q,j})_{int}\, e^{iq\theta}J_q(k_{q,j}r).$$

Plugging this in Equation (13) and isolating every mode gives:

$$\frac{da_{q,j}}{dt} = -\frac{ik_{q,j}^2}{2}a_{q,j} \qquad \forall\ (q,j)$$

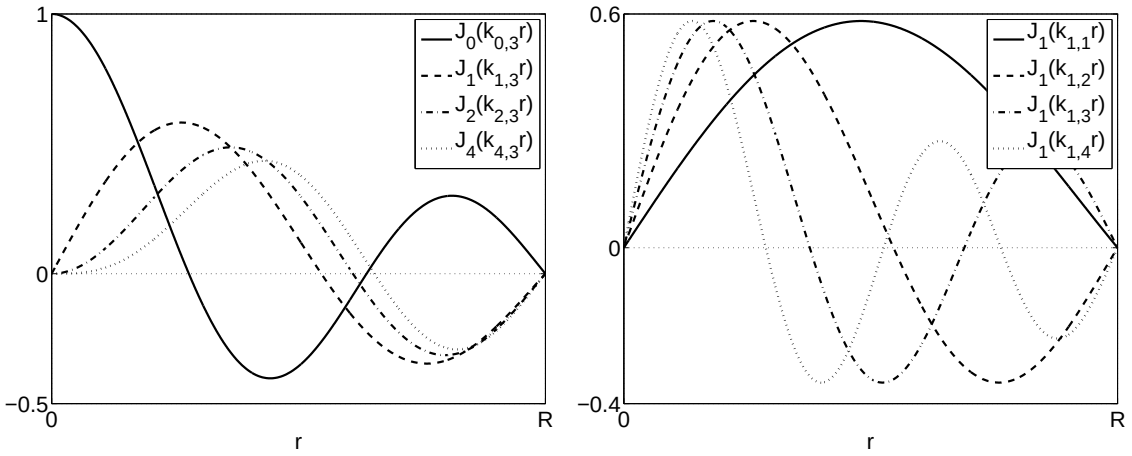

(a) (b)

Figure 3: (a) First four orders of the Bessel functions of the first kind, each of them scaled in order to have three zeros in $[0, R]$. (b) First four radial scalings of the Bessel function of the first kind of order 1.

and therefore, the integration from $(a_{q,j})_{int}$ to $a_{q,j}(t + dt)$ in a time step dt is exactly:

$$a_{q,j}(t + dt) = (a_{q,j})_{int} \exp\left(-\frac{ik_{q,j}^2 dt}{2}\right).$$

The recipe is then a classical one: go to the spectral space, integrate every coefficient $a_{q,j}(t)$ and go back to the physical space. It turns out that going to the spectral space and back is the most difficult part here. To isolate an azimuthal mode q, a Fourier transform of ψ_{int} in the azimuthal direction is performed, thanks to the orthogonality relation

$$\int_0^{2\pi} e^{-il\theta}\, e^{iq\theta} d\theta = 2\pi\delta_{ql},$$

δ_{ql} being the Kronecker symbol. Numerically, a FFT in the azimuthal direction is performed and no dealiaising is done. The output of the transform is then, for each $q \in \mathbb{Z}$:

$$\mathcal{F}[\psi_{int}]_q(r) = 2\pi \sum_{j=1}^{\infty} a_{q,j}(t) J_q(k_{q,j} r).$$

The radial modes described by the index j must now be isolated: the Fourier transform has isolated one order for the Bessel functions of the first kind, but not the different ways of scaling these function such that they would be zero in $r = R$. In other words, one has to isolate every function that is plotted in Figure 3(b), which is done using the following orthogonality relation:

$$\int_0^1 x J_q(\zeta_{q,j} x) J_q(\zeta_{q,p} x) dx = \frac{\delta_{jp}}{2} J_{q+1}^2(\zeta_{q,j}),$$

where $\zeta_{q,j}$ is the j^{th} zero of $J_q(x)$. By definition, $\zeta_{q,j} = k_{q,j}R$ and applying the variable change $r = Rx$, one gets the relation that is actually used for each j:

$$\int_0^R r J_q(k_{q,j}r) J_q(k_{q,p}r) dr = \frac{R^2 \delta_{jp}}{2} J_{q+1}^2(k_{q,j}R).$$

The corresponding operation performed on $\mathcal{F}[\psi_{int}]_q$ is a Hankel transform of order q, which is mathematically defined, for a function $f(x)$, as:

$$\mathcal{H}_q[f](k) = \int_0^{+\infty} x f(x) J_q(kx) dx.$$

In our case, we use a quasi-discrete Hankel transform (QDHT). The algorithm, exposed in detail and with clarity in [4], needs the input function to be evaluated at values of the radius $r_{q,j} = k_{q,j}R/k_{q,Y+1}$, where Y is the number radial modes that will be computed. This grid is specific to each q and we have to perform the QDHT for each one of them. It means that starting from an arbitrary ψ evaluated on a given grid, once this function has experienced a Fourier transform in the angular dimension, each projection on the azimuthal modes has to be interpolated on the grid $\{r_{q,j}\}$ with $1 \leq j \leq Y$ used by the QDHT of order q, which is a source of inaccuracy. The Matlab `spline` interpolation method has been chosen. Y has been chosen to be equal to half the number of points in the radial direction in order for the interpolation to be computed quite easily, the idea being that even for the highest radial modes, the oscillations of the Bessel function can be described by a few points between two zeros. This latter choice has not been the subject of any extensive study and shall be handled with care and suspicion.

We have isolated every (q, j) couples and are now in the spectral space. Before going back to the physical space, we just have to multiply every $(a_{q,j})_{int}$ by the propagator $\exp(-ik_{q,j}^2 dt/2)$. The next step is then to perform inverse quasi-discrete Hankel transforms (iQDHT) for each q, then re-interpolate the results back on the initial regular grid and finally perform an inverse FFT. We are now in the physical space with the function ψ evaluated at time $t + dt$.

3.3 Summary of the algorithm

Starting from $\psi(t)$, the different steps to get $\psi(t + dt)$ are:

1. multiply ψ by $\exp(i(1 - |\psi|^2)dt/2) \Rightarrow \psi_{int}$
2. perform a FFT of ψ_{int} along the azimuthal direction $\Rightarrow \mathcal{F}[\psi_{int}]_q$,
3. for each q, interpolate $\mathcal{F}[\psi_{int}]_q$ on the intermediate grid defined by $r_{q,j} = k_{q,j}R/k_{q,Y+1}$ with $1 \leq j \leq Y$,
4. for each q, perform the QDHT of order $m \Rightarrow \mathcal{H}_q[\mathcal{F}[\psi_{int}]_q]$,
5. for each (q, j), multiply $\mathcal{H}_q[\mathcal{F}[\psi_{int}]_q]$ by $\exp(-ik_{q,j}^2 dt/2) \Rightarrow \mathcal{H}_q[\mathcal{F}[\psi(t + dt)]_q]$,
6. for each q, perform the iQDHT of order q,
7. for each q, interpolate the previous results on the regular grid $\Rightarrow \mathcal{F}[\psi(t + dt)]_q$,
8. perform an iFFT of $\mathcal{F}[\psi(t + dt)]_q$ along the azimuthal modes direction $\Rightarrow \psi(t + dt)$.

4 Numerical experiments

4.1 General features of the settings

In all numerical experiments that are presented in this report, the radius of the glass is $R = 10$, the number of points in the radial and azimuthal directions are $n_r = n_\theta = 256$ and the number of radial modes is $Y = 128$, according to the rule we mentioned in Section 3.2. Initial conditions will all involve vortices put in a background particle density approximating a steady density distribution, as described in Section 2.3.1 for a different geometry. The function, approximating what the density distribution should be in the glass, is indeed inspired by the latter distribution, namely:

$$\psi_{bg}(r) = \tanh\left(\frac{R-r}{\sqrt{2}}\right).$$

The wave function of an isolated vortex of circulation $\Gamma = 2p\pi$ ($p \in \mathbb{Z}$) located in (r_0, θ_0) is approximated by:

$$\psi^v_{\{r_0;\theta_0;p\}}(r,\theta) = \frac{re^{ip\theta} - r_0 e^{ip\theta_0}}{\sqrt{1 + |re^{ip\theta} - r_0 e^{ip\theta_0}|^2}}.$$

It is now possible to generate various configurations involving vortices in a glass. For example, if one wants to generate an initial condition with one vortex of circulation $\Gamma = -2\pi$ located in $(R/2, 0)$ and one vortex of circulation $\Gamma = +4\pi$ located in $(R/8, \pi/2)$, the initial condition to set is:

$$\psi_0 = \psi_{bg} \times \psi^v_{\{R/2;0;-1\}} \times \psi^v_{\{R/8;\pi/2;2\}}.$$

Both definitions of ψ_{bg} and ψ^v are *approximations* of the background and vortices wave functions. The definition of ψ_{bg} will be more realistic for large values of R for instance, as it is inspired by a cartesian configuration with an infinitely long, plane wall. This will result in the generation of transients in the first moments of the simulations that can pollute the expected evolution of the system.

4.2 Conservation of the invariants

We will now check on a simple example if the three invariants N, E and L described in Section 2.3.2 are indeed conserved by our code. A property of the QDHT is to preserve the invariants but the use of the interpolations introduces errors, therefore the need to control if these errors are noticeable or not. We will set up an initial condition with one vortex:

$$\psi_0 = \psi_{bg} \times \psi^v_{\{3R/4;0;1\}},$$

as can be shown in Figure 4(a). Figure 4 in general shows how conserved are these quantities over a long period of time, a duration of more than 300 being three to four times longer than the experiments that will be shown later. We can see that N is only very slightly decreasing and that L and E both have a tendency to slightly decrease also, although they are subjected to oscillations. A possible explanation for these oscillations are that both of these quantities involve derivatives which are computed with the Matlab function `gradient` based on a rustic 2nd-order finite difference scheme. E is especially oscillatory and is in the

same time the function that includes the most derivatives, which is another hint that these oscillations might indeed be due to a rustic post-processing rather than a problem in the code.

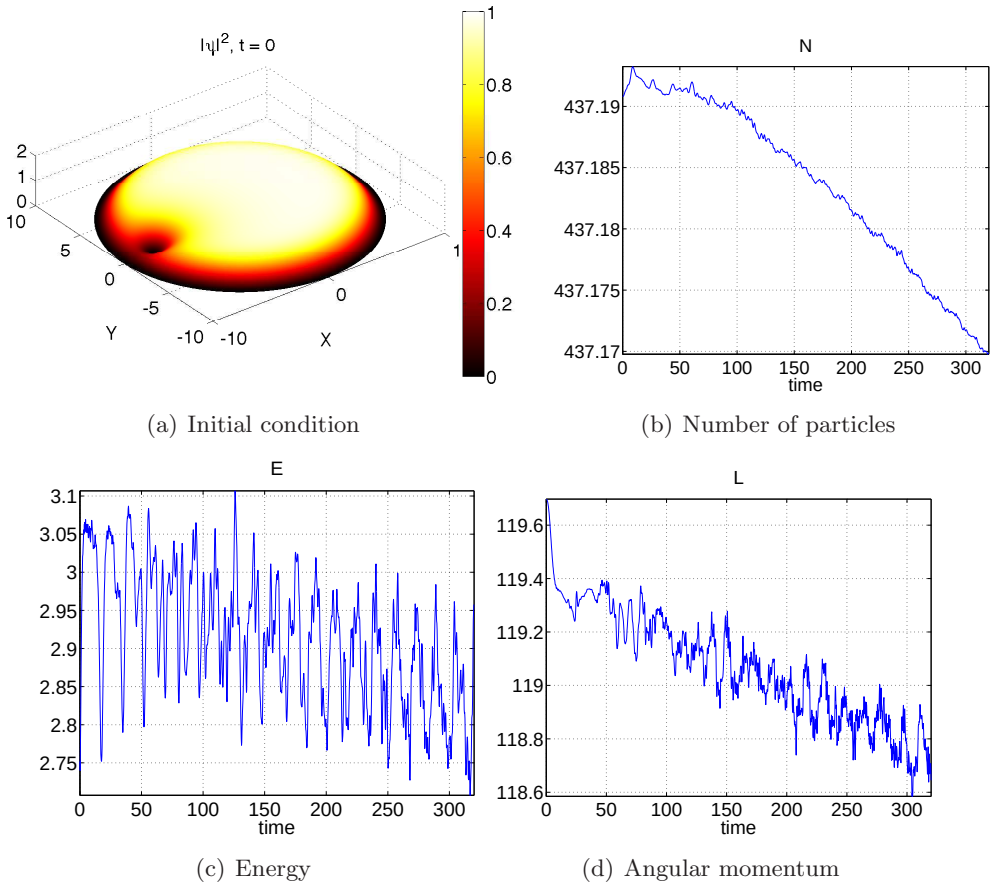

(a) Initial condition

(b) Number of particles

(c) Energy

(d) Angular momentum

Figure 4: Conservation of the three invariants N, E and L on an example with initial condition shown in (a). Although all curves seem to decrease, their value don't change much, as shown by the values displayed on the vertical axes.

Computing the invariants is a way to validate the accuracy of the code as to our knowledge, no analytical solution of simple problems exist in this geometry. We will now run numerical experiments to study simple problems that could be found in textbooks of classical fluid dynamics but that are uncharted territory in quantum fluid dynamics.

4.3 Vortex generation

We will see on a simple experiment that pair of vortices can be generated. It is hard to define an initial condition that would directly generate two vortices, so the following procedure has been applied: when two counter-rotating vortices are close to each other, they get closer and merge (see [2]). One can imagine then making two vortices merge, reversing the velocity field and plugging the resulting wave function in the NLS will later produce two

counter-rotating vortices. It is not that trivial as the NLS dynamics is not reversible (the time average of the field produced by any initial condition will eventually be proportional to ψ_{bg}). The procedure is then the following:

1. take an initial condition with two counter-rotating vortices:

$$\psi_0 = \psi_{bg} \times \psi^v_{\{R/8:0;1\}} \times \psi^v_{\{R/8;\pi;-1\}},$$

   and run the simulation for a duration of 10. As described in [2], the two vortices get closer, merge and disappear,

2. take the complex conjugate of the resulting wave function. By doing so, $\sqrt{n(t)}e^{i\alpha(t)} \mapsto \sqrt{n(t)}e^{-i\alpha(t)}$ and therefore $\boldsymbol{u} = \boldsymbol{\nabla}\alpha \mapsto \boldsymbol{u}' = -\boldsymbol{\nabla}\alpha = -\boldsymbol{u}$,

3. run again the simulation with the previous wave function as an initial condition for a duration of 20. Two vortices, almost exactly identical to the ones defined at the beginning of the first step of this procedure except with opposite circulation, appear and disappear again (see Figure 5).

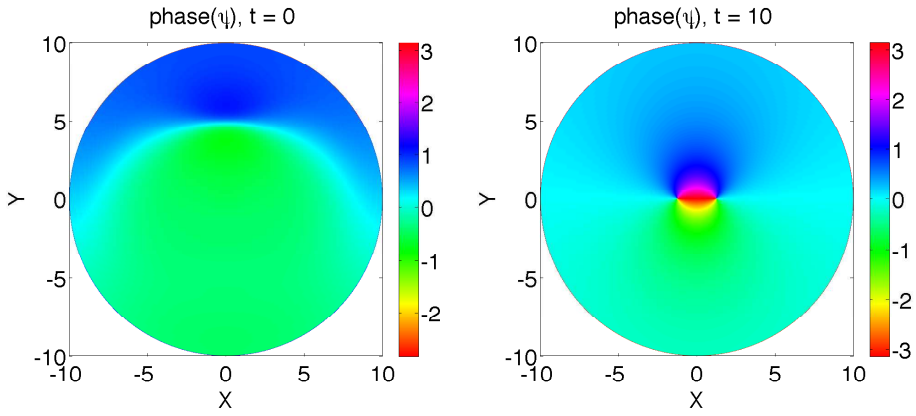

(a) (b)

Figure 5: Phase of the wave function for the generation of vortices. (a) Initial condition of step 2 in Section 4.3. (b) Vortices having been generated. We recall that the velocity is deduced from the phase by taking its gradient and that vortices are multi-valued points of the phase.

The vortices disappear shortly after having been generated. Nonetheless, we will see that the trajectory of a vortex can be modified, namely by a wave field in the numerical experiments shown in the rest of the present document. Therefore, a strong wave field could be able to separate two vortices and bring them far enough from each other such that they could behave like independent vortices. In the following studies, we will then focus on numerical experiments about one or two vortices of positive circulation[5].

[5] although considering isolated vortices in such a small glass ($R = 10$) is still unrealistic!

4.4 Initial vortex with double circulation

We design here an experiment with one vortex of double circulation at a distance $r_0 = 3R/4$ from the center:

$$\psi_0 = \psi_{bg} \times \psi^v_{\{3R/4;\pi;2\}}$$

(cf. Figure 6(a)) and let it run for a duration of 15. We see in Figure 6(b) that this vortex of double circulation has split into two vortices of simple circulation. Vortices of circulation higher than 2π in absolute value are therefore very likely to be unstable and in the next experiments, we will only consider vortices of simple circulation.

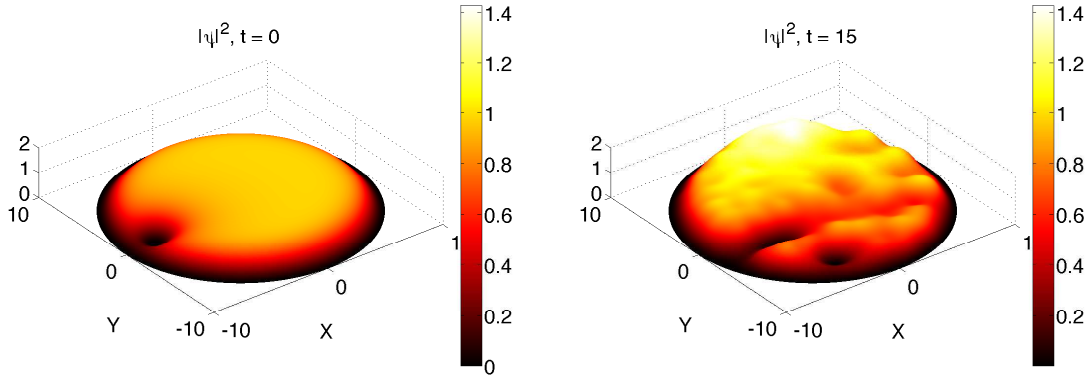

(a) Initial density

(b) Density after a little while

Figure 6: Initial and final density fields for an initial vortex of double circulation (a) which splits into two vortices of single circulation (b).

4.5 Motion of a single vortex

4.5.1 Method of images

In classical fluid dynamics, the motion of a point vortex near a wall is described by the method of images. In the case of a plane wall, the velocity field is the same as if there was no wall but instead a vortex of equal and opposite circulation and symmetrical position with respect to the wall, as sketched in Figure 7(a). In this case, the velocity induced by the virtual vortex and with which the vortex moves is parallel to the wall and equal to $\Gamma/4\pi b$, b being the distance to the wall. In the case of a vortex in a circular glass, the virtual vortex still has equal and opposite circulation but is now situated at a distance R^2/r_0 from the center of the glass, r_0 being the distance of the real vortex to the center (see Figure 7(b)). The velocity induced by it is again parallel to the wall and equal to $\Gamma r_0/2\pi(R^2 - r_0^2)$. The time for a vortex to loop around the entire box is then

$$\tau_{loop} = \frac{4\pi^2(R^2 - r_0^2)}{\Gamma}.$$

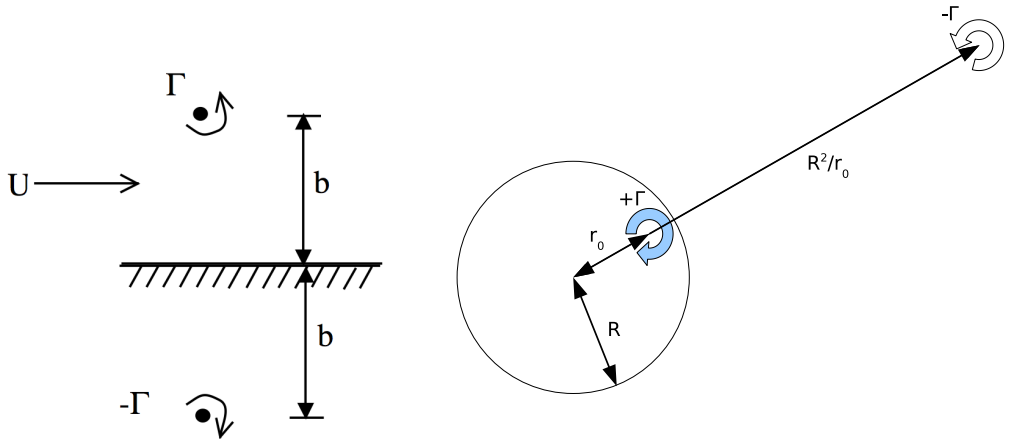

(a) Image vortices, plane wall (©2003 MIT, Dpt. of Ocean Engineering)

(b) Image vortices, circular glass

Figure 7: Sketch of the method of images for a vortex near a boundary in two different cases. In Figure (b), the blue vortex is real, the white one is virtual.

As explained in [6] in the case of a plane wall, this model has to include the boundary layer near the wall, which shifts the position of the wall. A way to understand it (rather than to prove it) is to consider a volume sketched in Figure 8, of arbitrary length and delimited by the wall and a line that is $\sqrt{2}$ away from the wall. The particle flux from the two lateral boundaries cancel each other as the system is invariant by translation along the wall and the particle flux through the wall is zero. The conservation of the number of particles tells that the particle flux has to be zero through the boundary facing the interior of the BEC. Within the healing length, the velocity is along the wall as the area is too confined to exhibit too complex structures, which means that there is no particle crossing this boundary either. The free-slip boundary condition that is necessary for the method of image vortices to be applied is therefore active *a healing length away* (times $\sqrt{2}$) from the wall. The correction in our case is then that the effective radius of the glass is $R' = R - \sqrt{2}$ and that the time for a vortex to loop around the glass is

$$\tau'_{loop} = \frac{4\pi^2((R-\sqrt{2})^2 - r_0^2)}{\Gamma}.$$

4.5.2 Numerical experiments

A series of numerical experiments has been performed with the same type of initial conditions as in Section 4.2, all starting from $\theta_0 = \pi$ where the initial distance to the wall has been varied. As displayed in Figure 9, the time for a vortex to make a loop is in general agreement with τ'_{loop}, whereas there is a systematic discrepancy with τ_{loop}. The model with correction is not valid in two cases. The first case is if the initial vortex position is too close to the wall, more precisely between the wall and the circle that is $\sqrt{2}$ away from the

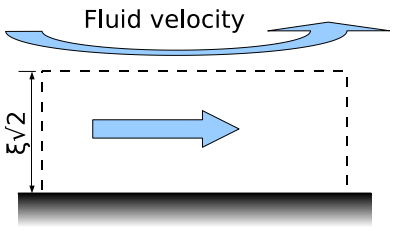

Figure 8: Sketch describing the effect of the boundary layer within the volume materialized by the dashed frame.

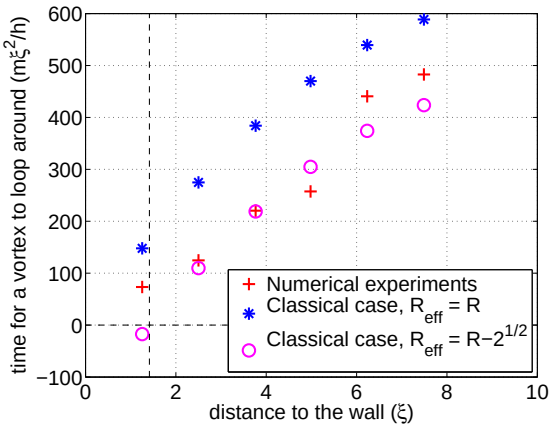

Figure 9: Measure of the time for a vortex to loop around the glass compared with the result provided by the image method with and without correction of the healing length for the effective radius R_{eff}. The vertical dashed line marks the virtual wall at $\sqrt{2}$.

wall, where the model with correction obviously doesn't apply. What happens, as shown in Figure 10(a) is that the vortex can even get "swallowed" in the wall if it is closer to it than $\sqrt{2}$. The second case is when the vortex is too close to the center. It then moves very slowly and is easily pushed by the wave field that has been generated mostly during the transient of the initial moments. As displayed in Figure 10(b), the course of the vortex is then erratic and again can't be described by the image vortex model.

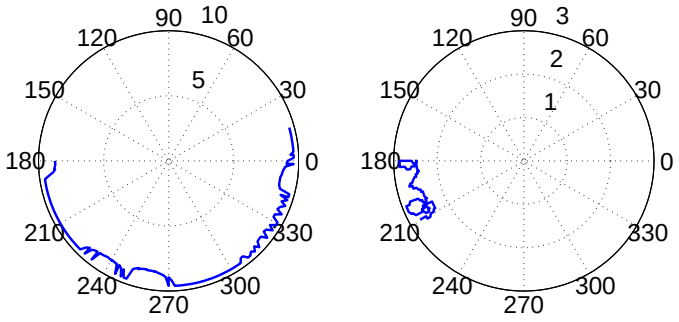

(a) $r_0 = R/4$ (b) $r_0 = 7R/8$

Figure 10: Trajectories of (a) a vortex, within the healing length, getting swallowed in the wall and (b) a vortex, far from the wall, being pushed by impulses due to the waves.

All experiments have been run for a duration of 40 and the time for a vortex to make a loop has been deduced from the angular velocity averaged over that period. An experiment starting from $r_0 = 3\pi/4$ has been run for a duration of 1570 (more than 12 loops), in order to determine if the vortex would get closer to the wall as it would propagate. This would mean that the vortex would lose energy, probably to the wave field. Even over such a long period of time, no shift in the distance to the wall has been observed.

4.6 Motion of two co-rotating vortices

In the case of two co-rotating vortices separated by a distance l, the velocity induced by one vortex at the location of the second one is $\Gamma/(2\pi l)$ and it then takes $\tau_{swap} = \pi^2 l^2/\Gamma$ for the two vortices to swap positions. An experiment is set up with two vortices of single circulation located symmetrically around the center of the box, as defined by

$$\psi_0 = \psi_{bg}(r,\theta) \times \psi^v_{\{R/4;0;1\}} \times \psi^v_{\{R/4;\pi;1\}},$$

as shown in Figure 11. In this case, the effect of the wall on each of these vortices has to be taken into account. Including the velocity induced by the other real vortex and the velocity induced by the virtual vortex of the corrected image method, the velocity of a vortex is

$$U = \frac{r_0}{(R-\sqrt{2})^2 - r_0^2} + \frac{1}{2r_0}$$

and the time for two vortices to swap positions is now

$$\tau'_{swap} = \frac{2\pi\, r_0^2 \left((R-\sqrt{2})^2 - r_0^2\right)}{(R-\sqrt{2})^2 + r_0^2} \approx 33.$$

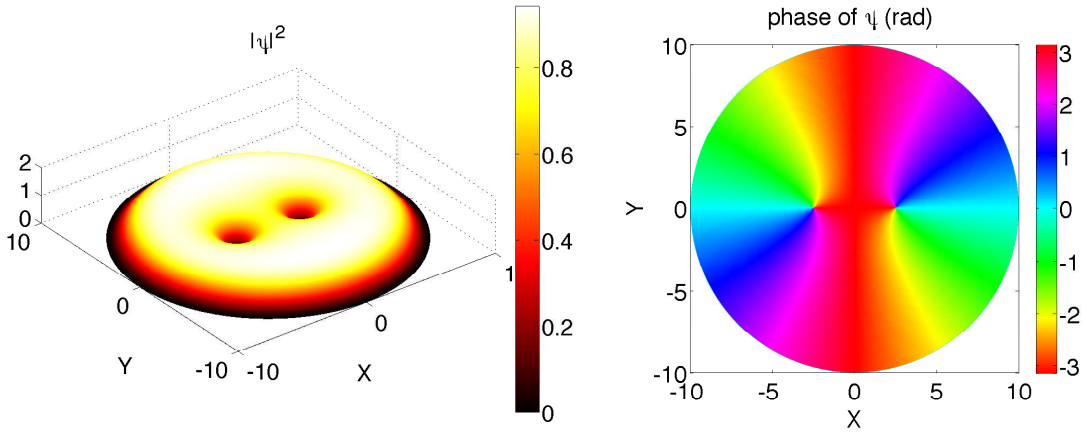

(a) Initial density

(b) Initial phase

Figure 11: Initial condition with two co-rotating vortices.

We run enough iterations for the two vortices to swap positions and just measure this duration. The measured time is $\tau'_{swap} = 53 \pm 1$, which is 1.6 times longer than the predicted duration. This discrepancy has not been explained yet, but one can notice that the vortices are quite close from each other and that the combined effects of what is going on in the depleted areas surrounding them might have to be taken into account.

5 Conclusion

The NLS equation governing quantum fluid dynamics can be transformed via the Madelung transformation in a set of equations resembling the set of shallow water, irrotational, compressible equations with surface tension. Quantum fluids support density waves behaving like capillary-gravity waves in shallow water and vortices are to be found where both real and imaginary parts of the wave function vanish on isolated points, making the phase of the wave function multi-valued and therefore singular. A novel method of integrating the NLS in polar coordinates, based on an operator-splitting method and the combination of FFTs in the azimuthal directions and quasi-discrete Hankel transforms in the radial direction, has been developed and partially validated. This allowed to do some physics in a quantum glass: we have seen that pair of vortices can be generated, justifying the existence of vortices in a non-rotating BEC and that to limit our study to vortices of single circulation $\Gamma = \pm 2\pi$ was fully relevant as vortices of double (and more) circulation were unstable and would split into vortices of simple circulation. We then saw that the motion of a single vortex has to take into account the presence of the depleted surface between the wall and the interior of the BEC which reduces the effective diameter of the glass. Finally, we saw that the motion of two co-rotating vortices that are close to each other noticeably departs from the classical case.

The possible extensions of this work are numerous and can be sorted into two categories. The first category involves the dynamics of BECs and more especially the interaction with

waves. We have seen here that it can modify the trajectory of a vortex and we infer that it can spearate freshly created vortices. We also infer that vortices can be peeled off a boundary by a wave field, as seen more of less convincingly in Figure 10(a) and that a vortex can lose energy by creating waves, which would lead to its location getting closer to the wall. To check the latter is especially challenging as it would require at least two things: first, to generate cleaner initial conditions for the shape of the wave function in a steady circular BEC and a cleaner profile for the shape of a vortex. Indeed, the approximateness of our ψ_{bg} and $\psi^v_{\{r_0;\theta_0;p\}}$ is the source of transients and of generation of waves, making it difficult to see if waves are generated when a vortex moves. Second, to see if the vortex will get closer after a while requires to run simulations for a while and then to be confident about the robustness of the code over long integrations, which brings us to the second category of extensions of the work, the numerics developed here: with the chosen time step, the code is stable but its duration can probably be optimized. The choice of n_r, n_θ and Y has not been optimized also and the exact effects of the interpolations on the precision and speed of the code remains unknown. De-aliaising has not been taken care of and in general, the performances of the method compared with other methods in polar coordinates are completely unknown.

Acknowledgements The staff of this 2009 GFD summer school is acknowledged, especially the two main lecturers Harvey Segur and Roger Grimshaw and the organisers Oliver Bühler, Karl Helfrich and Janet Fields. The company of the other fellows and undergraduates gravitating around Walsh Cottage made this summer an exceptionnal personal experience and I sincerely hope to be able to enjoy it for many years to come[6]. I also thank Pascale for her delicious brunches on Crooked Pond, George for sacrificing his patience to our softball skills[7] and Marcel Leutenegger for providing precious help in explaining how to use his Matlab Hankel transform toolbox. Last but not least, Oliver is warmly thanked again, this time for his supervision of this project, both efficient and full of humour.

References

[1] S. N. BOSE, *Plancks Gesetz und Lichtquantenhypothese*, Zeitschrift fuer Physik, 26 (1924), pp. 178–181. German translation of Bose's paper on Planck's law by Abert Einstein.

[2] O. BUHLER, *Wave–vortex interactions in fluids and superfluids.* In prep.

[3] K. B. DAVIS, M. O. MEWES, M. R. ANDREWS, N. J. VAN DRUTEN, D. S. DURFEE, D. M. KURN, AND W. KETTERLE, *Bose-einstein condensation in a gas of sodium atoms*, Phys. Rev. Lett., 75 (1995), pp. 3969–3973.

[4] M. GUIZAR-SICAIROS AND J. C. GUTIÉRREZ-VEGA, *Computation of quasi-discrete hankel transforms of integer order for propagating optical wave fields*, J. Opt. Soc. Am. A, 21 (2004), pp. 53–58.

[6] Long live the 6$^{\text{th}}$ Republic.

[7] Which existence has not yet been proved as we write.

[5] H. Lamb, *Hydrodynamics*, Cambridge Mathematical Library, Cambridge University Press, 6 ed., 1932, ch. VII, pp. 202–248.

[6] P. Mason, N. G. Berloff, and A. L. Fetter, *Motion of a vortex line near the boundary of a semi-infinite uniform condensate*, Physical Review A (Atomic, Molecular, and Optical Physics), 74 (2006), p. 043611.

[7] W. H. Press, B. P. Flannery, S. A. Teukolsky, and W. T. Vetterling, *Numerical recipes: the art of scientific computing*, Cambridge University Press, New York, NY, USA, 3 ed., 2007, ch. 20.3.3, pp. 1052–1053.